Published in final edited form as:

Arterioscler Thromb Vasc Biol. 2021 March ; 41(3): e160–e174. doi:10.1161/ATVBAHA.120.315875.

Inhibition of T-cells by cyclosporine A reduces macrophage accumulation to regulate venous adaptive remodeling and increase arteriovenous maturation

Yutaka Matsubara[1,2], **Gathe Kiwan**[1], **Jia Liu**[1], **Luis Gonzalez**[1], **John Langford**[1], **Mingjie Gao**[1], **Xixiang Gao**[1], **Ryosuke Taniguchi**[1,3], **Bogdan Yatsula**[1], **Tadashi Furuyama**[2], **Takuya Matsumoto**[4], **Kimihiro Komori**[5], **Alan Dardik**[1,6,7]

[1]Vascular Biology and Therapeutics Program, Yale School of Medicine, New Haven, CT

[2]Department of Surgery and Sciences, Kyushu University, Fukuoka, Japan

[3]Division of Vascular Surgery, The University of Tokyo, Tokyo, Japan

[4]Department of Vascular Surgery, Kyushu Central Hospital, Fukuoka, Japan

[5]Division of Vascular Surgery, Department of Surgery, Nagoya University Graduate School of Medicine, Nagoya, Japan

[6]Division of Vascular and Endovascular Surgery, Department of Surgery, Yale School of Medicine, New Haven, CT

[7]Department of Surgery, VA Connecticut Healthcare Systems, West Haven, CT

Abstract

Objective: Arteriovenous fistulae (AVF) are the preferred vascular access for hemodialysis but the primary success rate of AVF remains poor. Successful AVF maturation requires vascular wall thickening and outward remodeling. A key factor determining successful AVF maturation is inflammation that is characterized by accumulation of both T-cells and macrophages. We have previously shown that anti-inflammatory (M2) macrophages are critically important for vascular wall thickening during venous remodeling; therefore, regulation of macrophage accumulation may be an important mechanism promoting AVF maturation. Since CD4+ T-cells such as T-helper (Th) 1 cells, Th2 cells and regulatory T-cells (Treg) can induce macrophage migration, proliferation and polarization, we hypothesized that CD4+ T-cells regulate macrophage accumulation to promote AVF maturation.

Approach and Results: In a mouse aortocaval fistula model, T-cells temporally precede macrophages in the remodeling AVF wall. Cyclosporine A (CsA) (5mg/kg, sq, daily) or vehicle (5% dimethyl sulfoxide) was administered to inhibit T-cell function during venous remodeling. CsA reduced the numbers of Th1, Th2, and Treg cells, as well as M1- and M2-macrophage accumulation in the wall of the remodeling fistula; these effects were associated with reduced

Correspondence: Alan Dardik, Yale School of Medicine, 10 Amistad Street, Room 437, PO Box 208089, New Haven, CT 06520-8089 USA. Tel: 203-737-2082. alan.dardik@yale.edu.

Disclosures: None

vascular wall thickening and increased outward remodeling in wild-type mice. However, these effects were eliminated in nude mice, showing that the effects of CsA on macrophage accumulation and adaptive venous remodeling are T-cell-dependent.

Conclusion: T-cells regulate macrophage accumulation in the maturing venous wall to control adaptive remodeling. Regulation of T-cells during AVF maturation may be a strategy that can improve AVF maturation.

Graphical Abstract

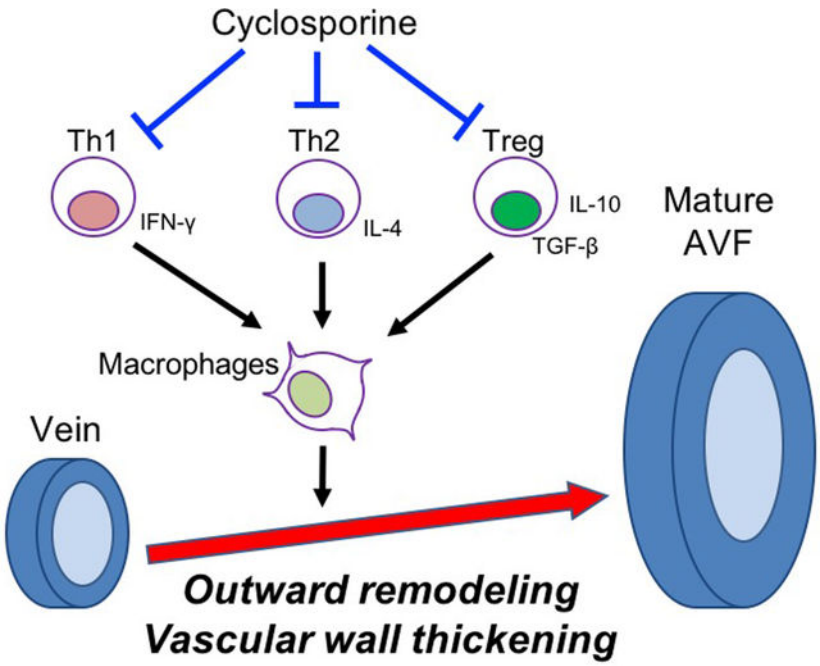

Keywords

Arteriovenous fistula; Cyclosporine A; T-cells; macrophages; inflammation

Subject terms

Basic Science Research; Inflammation; Vascular Biology

Introduction

More than 740,000 people in United States have end-stage renal disease and are treated with hemodialysis for renal replacement therapy[1]. Arteriovenous fistulae (AVF) are the preferred vascular access for hemodialysis because of the longer patency and fewer complications associated with AVF compared with grafts or catheters[2]. Successful use of an AVF is dependent upon venous adaptive remodeling to the fistula environment; primary AVF maturation requires venous wall thickening and outward remodeling[3]. However, the success rate of AVF maturation remains poor, with only approximately 30–50% of AVF successfully maturing and useable for hemodialysis within 6 months[4–6]. Therefore, the mechanisms of

venous wall thickening and outward remodeling are important to understand in order to improve the primary success rate of AVF maturation; for example, statins improve AVF maturation[7, 8], suggesting complex mechanisms that regulate venous adaptive remodeling.

Inflammation is an important factor regulating primary AVF maturation[9–15]. Venous remodeling requires inflammation that is characterized by the presence of both T-cells and macrophages in the remodeling venous wall[10, 16–19]. Macrophages are classically divided into 2 types, either inflammatory (M1) macrophages or anti-inflammatory (M2) macrophages[20]. Although the roles of M1-type macrophages in AVF maturation are still not well described, M2-type macrophages are required for venous wall thickening during AVF maturation[21, 22]; therefore, regulation of macrophage polarization may be an important mechanism enabling primary AVF maturation.

CD4+ T-cells, such as T-helper type 1 (Th1) cells, T-helper type 2 (Th2) cells and regulatory T-cells (Treg), can regulate macrophage polarization[23–25]. In particular, Th1 cells secrete interferon-γ (IFN-γ) to induce M1 macrophage polarization, Th2 cells secrete interleukin (IL)-4 to induce M2 macrophage polarization, and Treg secrete transforming growth factor-β (TGF-β) to induce M2 macrophage polarization[23–25]. We hypothesized that CD4+ T-cells secrete cytokines such as IFN-γ, IL-4 and TGF-β to induce macrophage polarization and enhance venous wall thickening, thereby promoting AVF maturation.

Cyclosporine A (CsA) is an immunosuppressive drug that inhibits T-cell function in both human patients and animal models[26–32]. Since CsA selectively inhibits T-cell proliferation, differentiation and cytokine production[33–36], we also hypothesized that CsA might reduce CD4+T-cell accumulation in the maturing AVF to regulate macrophage accumulation, thereby enhancing AVF maturation. Therefore, we determined whether inhibition of T-cells with CsA regulates macrophage accumulation to promote AVF maturation.

Materials and methods

The authors declare that all supporting data are available within the article [and its online supplementary files].

Mouse aortocaval fistula model.

All animal experiments were performed in strict compliance with federal guidelines and with approval from the Yale University IACUC. Wild type male and female C57BL6/J and athymic male NU/J mice 9–11 weeks of age were used; female mice have similar diameter increase and wall thickening as male mice through day 21 in this model[37]. Infrarenal aorto-caval fistulae were created as previously described[38]. Briefly, AVF were created by needle puncture from the aorta into the inferior vena cava (IVC) using a 25 G needle. Visualization of pulsatile arterial blood flow in the IVC was used to demonstrate technical success. Following surgery, all animals were monitored daily and evaluated weekly by a veterinarian for changes in health status.

Cyclosporine A treatment.

Cyclosporine A (CsA) (5 mg/kg; ab120114, Abcam) was delivered via subcutaneous injections starting on the day of the procedure and repeated daily throughout the study period. The control group received an equal volume of vehicle (5% dimethyl sulfoxide).

Measurement of fistula dilation.

Ultrasound (Vevo770 High Resolution Imaging System; Visual Sonics Inc., Toronto, Ontario, Canada; 40 MHz probe) was used to measure the diameter of the vessels as previously described[38, 39]. Ultrasound was performed prior to the operation (day 0 values) and serially post-operatively.

Histology.

The animals were euthanized and perfused with normal saline followed by 10% formalin via the left ventricle under physiologic pressure and the AVF was extracted en bloc. The tissue was then embedded in paraffin and cut in 5-μm cross sections. Elastin Van Gieson (EVG) staining was used to measure intima-media thickness, and trichrome and picrosirius red stains were used to measure collagen density in 5 μm cross sections of the IVC using sections obtained 50–100 μm cranial to the fistula. Eight equidistant points around the IVC wall were averaged in each cross section to obtain the mean AVF outer wall thickness and collagen density[21]. Additional unstained cross sections in this same region were used for immunohistochemistry and immunofluorescence microscopy.

Immunohistochemistry.

Tissue sections were de-paraffined using xylene and a graded series of ethanol. For antigen-retrieval, sections were heated in citric acid buffer (pH 6.0) at 100˚C for 15 minutes. Non-specific background staining of endogenous peroxidase was treated with 0.3% hydrogen peroxide for 30 minutes, and sections were blocked with 3% bovine serum albumin in PBS (pH 7.4) for 1 hour at room temperature. Sections were then incubated at 4˚C with the primary antibody (Major Resources Table). After overnight incubation, the sections were incubated with HRP conjugated secondary antibody for 1 hour at room temperature and treated with Dako Liquid DAB+ Substrate Chromogen System (GV825, Agilent Dako) to detect the reaction products. Finally, the sections were counterstained with Dako Mayer's Hematoxylin (Lillie's Modification) Histological Staining Reagent (S3309, Agilent Dako). For negative controls for the antibodies, IgG isotype controls, negative tissue controls and endogenous tissue background controls were used.

Immunofluorescence.

Tissue sections were de-paraffined and then heated in citric acid buffer (pH 6.0) at 100˚C for 15 minutes for antigen retrieval. The sections were blocked with 3% bovine serum albumin prior to incubation with primary antibodies (Major Resources Table) overnight at 4˚C. After incubation, the sections were incubated with Alexa Fluoro secondary antibodies for 1hour and stained with 4',6-diamidino-2-phenylindole (DAPI) (P36935, Invitrogen) to stain cellular nuclei. Positively staining cells were counted per high power fields. For negative

controls for the antibodies, IgG isotype controls, negative tissue controls and endogenous tissue background controls were used.

Western Blot and cytokine array.

The entire IVC was removed with care taken to avoid surrounding arterial and connective tissues. Proteins were extracted with RIPA lysis buffer containing protease inhibitors from single IVC[21, 40]. Protein concentrations were assessed using a colorimetric assay (Bio Rad), and equal amounts of protein were run on a sodium dodecyl sulfate polyacrylamide gel electrophoresis gel and then transferred to a polyvinylidene difluoride membrane. After blocking with 5% skim milk, membranes were probed overnight with the primary antibodies (Major Resources Table). After overnight incubation, the membranes were incubated with HRP conjugated secondary antibodies for 1 hour at room temperature and were developed with using Western Lightning Plus ECL reagent (NEL105001EA, PerkinElmer; Waltham, MA). Lysates were also examined with a cytokine array using the Mouse Neuro Antibody Array kit (ab211069, Abcam) according to the instructions for use.

RNA Extraction and Real-Time Quantitative Polymerase Chain Reaction.

The entire IVC was removed with care taken to avoid surrounding arterial and connective tissue. Total RNA was isolated from these samples by using RNeasy Mini Kit (74106, Qiagen; Valencia, CA). RNA quality was confirmed using a NanoDrop spectrophotometer (Thermo Scientific; Wilmington, DE) to determine the 260/280 nm ratio. Reverse transcription was performed using SuperScript III First-Strand Synthesis Supermix (11752250, Invitrogen). Real-time PCR was performed using iQ SYBR Green Supermix (1708880, Bio-Rad) and amplified for 40 cycles using the iQ5 Real-Time PCR Detection System (Bio-Rad). Primers are summarized in Major Resources Table. All samples were normalized to GAPDH amplification and graphed in arbitrary units.

Lymphocyte collection.

Mouse spleens were harvested from C57BL/6J mice and minced in PBS. The cell suspension was filtered through 50μm cell strainers and loaded on the top of the lymphocyte separation medium (1077, Promo Cell; Heidelberg, Germany) and centrifuged at 440g for 30 minutes. Lymphocytes were collected from the mononuclear cell layer. After washing the cell suspension with PBS, cell numbers were adjusted to 10^6 cells/ml.

In vitro T-cell proliferation, migration and cytokine production assays.

Anti-mouse CD3 antibody (MAB4841, R&D systems; 1 μg/ml dilution) was loaded into each well of a 96-well plate and coated on the well bottoms overnight at 4˚C. Lymphocytes were incubated at 37˚C in the CD3 antibody-coated 96-well plate in RPMI/10%FBS with CsA (0.1μg/ml) or the same amount of vehicle (5% dimethyl sulfoxide). Cell numbers were counted to assess cell proliferation. After 24-hour incubation, cells and cell supernatant were collected for the migration assay and cytokine measurements, respectively. The migration assay was performed using the CytoSelect 96-Well Cell Migration Assay (CBA-105, Cell Biolabs; San Diego, CA) according to the instructions for use. Cytokines in the cell

supernatant were measured using IL-2 (M2000, R&D systems) and IFN-γ (MIF00, R&D systems) ELISA kits according to the instructions for use.

Statistics.

Data are represented as mean value ± SEM. All data were analyzed using Prism 8 software (GraphPad Software, Inc., La Jolla, CA). Normality was confirmed using the Shapiro-wilk test. Statistical significance was determined using Student's t-test or ANOVA with Sidak's post hoc correction. We used the Mann-Whitney U test or the Kruskal-Wallis test with Dunn's post hoc correction if the sample size was smaller than 6. P values < 0.05 were considered significant.

Results

T-cells and macrophages accumulate during venous remodeling in wild type mice

To determine a role for T-cells and macrophages during venous adaptive remodeling, we examined AVF maturation in a mouse model at day 7, prior to the establishment of a thickened venous wall and when inflammatory cells have been observed[21, 22]. To confirm the accumulation of T-cells and macrophages during venous remodeling, we performed Western blot (Figure 1A), immunohistochemistry (Figure 1B) and qPCR (Figure 1C) analyses to determine the presence of CD3 or CD68. Western blot showed significantly increased CD3 and CD68 immunoreactivity in the AVF (Figure 1A). Immunohistochemistry showed significantly increased accumulation of CD3+ cells and CD68+ cells throughout the AVF wall (Figure 1B). qPCR showed significantly increased CD3 and CD68 mRNA in the AVF (Figure 1C). These findings show that T-cells and macrophages accumulate in the remodeling venous wall during AVF maturation. Immunohistochemistry also confirmed the presence of IL-2 and IFN-γ, cytokines that are produced by T-cells, in the remodeling venous wall (Figure 1D), suggesting that the T-cells may be functional. To determine if other cytokines are present during venous remodeling, we performed a cytokine array examining the IVC wall derived from mice 7 days after a sham or an AVF procedure (Figure 1E); there were significant increases in immunoreactivity of TGF-β, monocyte chemotactic protein −1 (MCP-1), lipopolysaccharide-induced CXC chemokine (LIX) and IFN-γ in the AVF (Table 1), all of which were also present in the AVF wall (Figure 1F). These findings show that T-cells and macrophages accumulate in the remodeling venous wall and suggest that inflammation may have important roles during AVF maturation.

T-cells precede macrophages in the remodeling venous wall in wild type mice

We have previously shown that the mouse aortocaval fistula model recapitulates human AVF maturation, with venous adaptive remodeling occurring during postoperative days 0 to 21[39]. To determine the time course of T-cell and macrophage presence in the remodeling venous intima, media and adventitia, we used immunofluorescence to examine the AVF wall for CD3- and CD68-positive cells at days 0, 3, 7 and 21 (Figure 2A and Supplemental figure IA). Accumulation of both T-cells and macrophages in the venous intima, media and adventitia was significantly increased at days 3 and 7; however, T-cells had maximal accumulation in the AVF wall at day 3, prior to maximal accumulation of the macrophages at day 7 (Figure 2B), suggesting that T-cells may regulate macrophage accumulation during

venous remodeling. Since Th1, Th2 and Treg have important roles to stimulate macrophage differentiation, polarization and proliferation, we determined the presence of CD4+/IFN-γ+ (Th1), CD4+/IL-4+ (Th2) and CD4+/Foxp3+ (Treg) dual-positive cells in the venous intima, media and adventitia (Figure 2C and Supplemental figure IB–D). There was significant accumulation of Th1 (Figure 2D), Th2 (Figure 2E) and Treg (Figure 2F) cells in the AVF at day 3, suggesting that Th1, Th2 and Treg T-cells may stimulate macrophage differentiation, polarization and/or proliferation during adaptive venous remodeling.

Cyclosporine A is associated with reduced T-cells and macrophages during venous remodeling in wild type mice

Since Th1, Th2 and Treg regulate macrophage differentiation, polarization and proliferation, we hypothesized that inhibition of Th1, Th2 and Treg would reduce macrophage accumulation during venous remodeling. We injected vehicle or CsA (5 mg/kg; subcutaneously) during the entire AVF maturation phase to inhibit T-cell function. Mouse serum CsA concentration was within the clinically effective range (Supplemental Figure IIA) without any adverse effects on renal function (Supplemental Figure IIB, IIC); there was no change in postoperative survival rate (Supplemental Figure IID) or change in body weight (Supplemental Figure IIE). We also examined CD3 in mouse spleens to determine the effects of CsA on T-cells in a second location besides the AVF; as expected, CsA significantly reduced CD3 mRNA expression in mouse spleens (Supplemental Figure IIF).

In the remodeling venous intima, media and adventitia, CsA was associated with reduced numbers of CD3+/CD4+ dual-positive cells (CD4+T-cells) as well as CD3+/CD8+ dual-positive cells (CD8+T-cells) (Figures 3A–C and Supplemental figure IIIA, IIIB). To confirm which subsets of CD4+T-cells were reduced by CsA, we performed immunofluorescence of the AVF venous intima, media and adventitia in mice treated with vehicle or CsA (Figure 3D and Supplemental figure IIIC–E); CsA significantly reduced accumulation of CD4+/IFN-γ (Th1), CD4+/IL-4 (Th2) and CD4+/Foxp3 (Treg) cells (Figure 3E–G). Similarly, CsA reduced accumulation of CD8+/CCR7+ (naive CD8+) T-cells (Figure 3H–I and Supplemental figure IIIF); however, there were few CD8+/CCR7- (cytotoxic) T-cells in the AVF venous intima, media and adventitia without significant differences between vehicle and CsA (Figure 3J). These findings show that CsA reduced accumulation of Th1, Th2, and Treg cells during venous remodeling; however, CsA did not affect accumulation of active CD8+T-cells.

To determine if CsA reduced cytokine secretion by T-cells, we measured secreted IL-2 and IFN-γ, cell proliferation and cell migration in T-cells treated with vehicle or CsA in vitro. CsA inhibited secretion of IL-2 (Supplemental Figure IIIG) and IFN-γ (Supplemental Figure IIIH) as well as T-cell proliferation (Supplemental Figure IIII); however, CsA did not inhibit T-cell migration (Supplemental Figure IIIJ) in vitro. These results show that CsA inhibits cytokine production and T-cell proliferation, but not T-cell migration, in vitro, consistent with the effects observed in vivo (Figures 3A–J).

Since Th1, Th2 and Treg have important roles in regulating macrophage differentiation, polarization and proliferation, we hypothesized that inhibition of Th1, Th2 and Treg would reduce macrophage accumulation during venous remodeling. CsA was associated with

reduced numbers of CD68+/interferon-γ receptor (IFNR)+ (M1), CD68+/inducible nitric oxide synthase (iNOS)+ (M1), CD68+/ transglutaminase 2 (TGM2)+ (M2) and CD68+/ CD206+ (M2) dual-positive cells in the AVF venous intima, media and adventitia (Figures 3K–O and Supplemental figure IIIK–N). There were no significant differences in the M2:M1 macrophage ratio between the groups (Figure 3P), suggesting that CsA reduced accumulation of both M1-type and M2-type macrophages in the remodeling AVF wall. Since CsA reduced accumulation of both T-cells and macrophages, we determine if CsA reduces vascular cell adhesion molecule 1 (VCAM1) expression in the vascular endothelium; CsA significantly reduced VCAM1 expression in vascular endothelial cells (Figure 3Q and Supplemental figure IIIO). In toto, these data show that CsA reduces accumulation of Th1, Th2, and Treg T-cells, as well as M1- and M2-type macrophages, reducing the inflammatory response in the vascular wall during venous remodeling.

Cyclosporine A reduces AVF wall thickening but promotes outward remodeling in wild type mice

Since macrophages promote venous wall thickening during adaptive remodeling[21, 22], we next determined whether the reduced macrophage accumulation associated with CsA treatment was also associated with reduced thickness of the AVF walls. CsA treatment was associated with significantly thinner AVF walls, compared with vehicle alone, at day 21 (Figure 4A), in both male as well as in female mice (Supplemental figure IVA). Since smooth muscle cell (SMC) proliferation leads to vascular wall thickening during AVF maturation, we determined the effects of CsA on SMC proliferation and apoptosis (Figure 4B and Supplemental figure IVB–D); CsA significantly reduced SMC proliferation (Figure 4C) but there were no detectable apoptotic cells (Figure 4D). Since Akt signaling has important roles in SMC proliferation during venous remodeling to promote vascular wall thickening[22, 41], we assessed Akt phosphorylation in the maturing AVF (Figure 4E–F and Supplemental figure IVE). CsA treatment was associated with significantly reduced phospho-Akt in the AVF wall (Figure 4E), with reduced phospho-Akt in α-actin positive cells (Figure 4F and Supplemental figure IVE). These data show that CsA treatment is associated with reduced SMC proliferation and Akt phosphorylation, as well as reduced vascular thickening, during venous remodeling.

Since macrophages also have important roles in collagen production during vascular remodeling, we determined collagen density in the vascular wall of maturing AVF treated with vehicle or CsA (Figure 5A). CsA was associated with significantly reduced collagen density at days 7 and 21 (Figure 5B–C), with reduced density of collagen I but not collagen III (Figure 5D–F). Since TGF-β1 regulates collagen production during vascular remodeling[42], we determined if CsA was associated with altered TGF-β1 expression during AVF maturation; CsA treatment was associated with significantly fewer numbers of TGF-β1+ cells (Figure 5G and Supplemental figure VA). There was no significant difference in MMP-9 immunoreactivity between control and CsA-treated AVF (Supplemental figure VB). Since collagen is an important component of the extracellular matrix that maintains vascular wall strength, we hypothesized that the reduced collagen density associated with CsA treatment would enhance outward remodeling. We used ultrasound to determine the diameter of the AVF as it undergoes adaptive remodeling; CsA was associated with

significantly increased outward remodeling (Figure 5H and Supplemental figure VC) resulting in improved blood flow (Figure 5I) without significant differences in wall shear stress (Supplemental Figure VD). Similar trends were observed in female mice (Supplemental Figure VE–G). These data show that CsA treatment is associated with reduced TGF-β1 expression and collagen production, as well as enhanced outward adaptive remodeling.

CsA effects on macrophage accumulation and adaptive remodeling are T-cell-dependent

To determine whether CsA-reduced macrophage accumulation, VCAM expression, SMC proliferation, Akt phosphorylation and TGF-β expression are dependent on T-cells, we used a genetic approach and treated athymic nude mice (NU/J) with vehicle or CsA after surgical creation of an AVF. We first confirmed absence of mature T-cells in the AVF wall in athymic nude mice (Figure 6A). As expected, there were no CD3+CD4+ T-cells, CD3+CD8+ T-cells or IL-2+ cells in the AVF in nude mice (Figure 6A and Supplemental Figure VIA–C). Although CsA reduced both M1- and M2-macrophage accumulation in the AVF created in wild type mice (Figure 3K–O), there were no significant differences in M1 and M2 macrophage accumulation in the AVF created in athymic nude mice (Figure 6B–F and Supplemental figure VID–G), suggesting that the CsA-reduced macrophage accumulation during venous remodeling is dependent on T-cells. We also assessed the immunoreactivity of endothelial VCAM1, SMC ki67, SMC phospho-Akt and SMC TGF-β1 (Figure 6G and Supplemental figure VIH–K) in athymic nude mouse AVF, all of which were significantly reduced by CsA in wild type mouse AVF (Figure 3P, 4B–C, 4E–F, 5G); however, in athymic nude mice treated with vehicle or CsA, there were no significant differences in VCAM1 (Figure 6H), ki67 (Figure 6I), cleaved caspase 3 (Supplemental Figure VIL), phospho-Akt (Figure 6J) and TGF-β1 (Figure 6K) in the AVF walls, suggesting that the reduced immunoreactivity in wild type mice (Figure 3) is dependent on T-cells.

In addition, there were no significant differences in wall thickening (Figure 7A–B) and collagen density (Figure 7A, 7C–D) in the AVF wall of athymic nude mice treated with vehicle or CsA. Since collagen I density was reduced in the AVF walls of wild type mice treated with CsA (Figure 5), we also assessed collagen I density in nude mouse AVF treated with vehicle or CsA; there was no significant difference in collagen I density between vehicle and CsA (Figure 7E). Since reduced collagen density was associated with increased outward remodeling in the AVF of wild type mice (Figure 5), we used ultrasound to determine the diameter of the AVF of nude mice during adaptive remodeling during AVF maturation; there was no significant difference in outward remodeling in nude mice treated with vehicle or CsA (Figure 7F). These data show that CsA-reduced vascular wall thickening and collagen density associated with increased outward remodeling are dependent on T-cells, that is adaptive remodeling during AVF maturation is T-cell-dependent.

Discussion

We show that T-cells temporally precede macrophages in the remodeling venous wall (Figure 2A) and that CsA reduced Th1, Th2, and Treg cells, as well as M1- and M2-

macrophage accumulation in the wall of the maturing AVF (Figure 3); these effects are associated with reduced vascular wall thickening and increased outward remodeling in wild-type mouse AVF (Figure 4A, 5H). However, these effects were eliminated in nude mouse AVF (Figure 6–7), showing that the effects of CsA on macrophage accumulation and adaptive venous remodeling are T-cell-dependent. These results suggest that T-cells regulate macrophage accumulation in the maturing venous wall to control adaptive remodeling.

AVF maturation requires inflammation that is characterized by accumulation of T-cells and macrophages[18, 21, 22, 41]. We previously showed that systemic inhibition of inflammation with clodronate results in AVF failure[22], suggesting the need to regulate inflammation more specifically, perhaps via targeting of M1- macrophages, M2-macrophages or T-cells. Macrophages are classically divided into M1 or M2 macrophages, and we have previously shown that M2 macrophages are critical for venous adaptive remodeling[21]. In this study, we confirmed these findings and showed that reduced M2 macrophages were associated with less vascular wall thickening that was associated with SMC proliferation but not apoptosis (Figure 3K–O, 4A–D), similar to our previous results[42]. CD4+ T-cells such as Th1, Th2 and Treg cells have critical roles to regulate M2 macrophages; for example, Th1 secrete IFN-γ to induce M1 macrophage polarization, Th2 secrete IL-4 to induce M2 macrophage polarization and Treg secrete TGF-β1 to induce M2 macrophage polarization[23–25]. We showed increased IFN-γ, TGF-β1, LIX-1 and MCP-1 in the adapting venous wall (Figure 1D–F and Table), consistent with accumulation of functional T-cells and macrophages in the maturing AVF. We also showed that T-cells precede macrophages in the maturing AVF wall (Figure 2), and inhibition of T-cells reduced macrophage accumulation (Figure 3). These findings suggest that T-cells are necessary for macrophage accumulation in the AVF wall. We do not clarify whether circulating T-cells infiltrated or resident T-cells proliferated in the remodeling AVF wall; additional analysis such as bone marrow ablation or adoptive transfer experiments could help clarify from where the T-cells originate. Reduced numbers of T-cells in the venous wall were associated with reduced collagen production that promoted outward remodeling (Figure 3A–J, 5), and TGF-β1 plays an important role in collagen production during venous remodeling (Figure 5)[42]. Since Treg cells are associated with TGF-β1 production[43, 44], reduced Treg cells might be associated with reduced TGF-β1 in the venous wall to inhibit collagen production. Although MMP are associated with collagenolysis[45], MMP-2,MMP-3 and MMP-9 expression were not changed (Figure 1E, Supplemental figure VB and Table); since MMP are produced by macrophages whose presence is reduced by CsA, we believe that the reduced collagen expression with CsA is less likely to be mediated by MMP and more likely due to reduced TGF-β activity (Figure 5G).

CD4+ T-cells are required to maintain proper blood flow and lumen area in a rat AVF model; however, the association between CD4+ T-cells and macrophage accumulation was not described[19]. Our data show the importance of CD4+ T-cells during venous adaptive remodeling and that Th1, Th2 and Treg cells regulate macrophage accumulation to enhance AVF maturation. Although we did not show the significance of LIX1 and MCP-1 that are significantly increased in the adapting venous wall (Figure 1E–F, Table), LIX1 and MCP-1 may also have important roles, as they are macrophage-associated cytokines.

CsA is in clinical use for patients after organ transplantation and patients with autoimmune diseases[26–28]. CsA selectively blocks T-cell proliferation, differentiation and cytokine production[33–36]. Similarly, our in vitro data show that CsA inhibits T-cell proliferation and production of IFN-γ and IL-2 (Supplemental figure IIIGH). Since IL-2 and IFN-γ are necessary to activate other inflammatory cells including macrophages[23–25], CsA indirectly inhibits inflammatory cells that are activated by T-cells[46]. Our data show that CsA reduced macrophage accumulation to enhance adaptive venous remodeling in wild-type mice (Figure 3–5) but not in nude mice (Figure 6, 7). These data show that the effects of CsA on adaptive venous remodeling such as SMC proliferation and collagen production depend on T-cells, since nude mice do not have CD3+T-cells including Th1, Th2 and Treg.

CsA has several effects during vascular remodeling including promotion of endothelial dysfunction and vasoconstriction, independent of its effects on T-cells[29–32]; however, we did not observe any adverse effects of CsA in this study (Supplemental figure II). The effects of CsA are dose-dependent[47], suggesting that there is an optimal dose of CsA to improve AVF maturation. Although we assessed only a single dose (5mg/kg) of CsA, additional studies might show an optimal dose of CsA that maximizes outward remodeling to promote fistula maturation. In addition, we assessed only male mice; since there are sex differences in immunity, it is important to assess the effects of CsA in female mice to understand the translational significance of this potential therapy.

This study has several limitations. We assessed only healthy mice; although our mouse model of adaptive remodeling recapitulates human AVF maturation[39], human patients have comorbidities such as chronic kidney disease, hypertension and diabetes that alter inflammation and thus could affect AVF maturation. Assessments of AVF maturation in mice with chronic kidney disease would be relevant; however, experiments on mice with chronic kidney disease are challenging because of their poor survival rate in surgical models that may predispose the data to survival bias[48, 49]. Although we assessed only healthy mice, nevertheless we believe that T-cells have important roles during human AVF maturation since human studies have shown the presence of T-cells in the AVF wall[50, 51]. Finally, although our data shows similar effects of CsA in female mice compared to male mice (Supplemental Figure IVA, VE–G), this data does not fully explore potential sex differences in T-cell function during AVF maturation; other studies have shown several sex differences in AVF maturation[37, 52].

Although inhibition of T-cells reduced vascular wall thickening that is required for AVF maturation, the most common cause of human AVF failure is lack of outward remodeling[2], The novel finding of this study is that inhibition of T-cells promoted outward remodeling and blood flow, and thus suggesting that T-cells may be a novel target to promote outward remodeling during AVF maturation. In summary, inhibition of T-cells promotes outward remodeling and inhibits vascular wall thickening during adaptive remodeling. Regulation of T-cells during AVF maturation may be a strategy that can improve AVF maturation

Supplementary Material

Refer to Web version on PubMed Central for supplementary material.

Sources of funding:

This work was supported by US National Institute of Health (NIH) grant R01-HL144476 [to A.D.] and the Uehara Memorial Foundation postdoctoral fellowship [to Y.M.] as well as with the resources and the use of facilities at the VA Connecticut Healthcare System, West Haven, CT.

Abbreviations

AVF	arteriovenous fistula
CsA	Cyclosporine A
DAPI	4’,6-diamidino-2-phenylindole
EVG	elastin van Gieson
IFN-γ	interferon-γ
IFNR	interferon-γ receptor
IL	interleukin
iNOS	inducible nitric oxide synthase
IVC	inferior vena cava
LIX	lipopolysaccharide-induced CXC chemokine
MCP-1	monocyte chemotactic protein −1
SMA	smooth muscle actin
SMC	smooth muscle cell
Th1	T-helper type 1 cells
Th2	T-helper type 2 cells
Treg	regulatory T-cells
TGF-β	transforming growth factor-β
VCAM1	vascular cell adhesion molecule 1

References

1. Saran R, Robinson B, Abbott KC, et al. Us renal data system 2017 annual data report: Epidemiology of kidney disease in the united states. Am J Kidney Dis. 2018;71:A7 [PubMed: 29477157]
2. Disbrow DE, Cull DL, Carsten CG 3rd, Yang SK, Johnson BL, Keahey GP. Comparison of arteriovenous fistulas and arteriovenous grafts in patients with favorable vascular anatomy and equivalent access to health care: Is a reappraisal of the fistula first initiative indicated? J Am Coll Surg. 2013;216:679–685; discussion 685–676 [PubMed: 23395157]
3. Hu H, Patel S, Hanisch JJ, Santana JM, Hashimoto T, Bai H, Kudze T, Foster TR, Guo J, Yatsula B, Tsui J, Dardik A. Future research directions to improve fistula maturation and reduce access failure. Semin Vasc Surg. 2016;29:153–171 [PubMed: 28779782]

4. Al-Jaishi AA, Oliver MJ, Thomas SM, Lok CE, Zhang JC, Garg AX, Kosa SD, Quinn RR, Moist LM. Patency rates of the arteriovenous fistula for hemodialysis: A systematic review and meta-analysis. Am J Kidney Dis. 2014;63:464–478 [PubMed: 24183112]
5. Allon M, Lockhart ME, Lilly RZ, Gallichio MH, Young CJ, Barker J, Deierhoi MH, Robbin ML. Effect of preoperative sonographic mapping on vascular access outcomes in hemodialysis patients. Kidney Int. 2001;60:2013–2020 [PubMed: 11703621]
6. Dixon BS, Novak L, Fangman J. Hemodialysis vascular access survival: Upper-arm native arteriovenous fistula. Am J Kidney Dis. 2002;39:92–101 [PubMed: 11774107]
7. Janardhanan R, Yang B, Vohra P, Roy B, Withers S, Bhattacharya S, Mandrekar J, Kong H, Leof EB, Mukhopadhyay D, Misra S. Simvastatin reduces venous stenosis formation in a murine hemodialysis vascular access model. Kidney Int. 2013;84:338–352 [PubMed: 23636169]
8. Cui J, Kessinger CW, Jhajj HS, Grau MS, Misra S, Libby P, McCarthy JR, Jaffer FA. Atorvastatin reduces in vivo fibrin deposition and macrophage accumulation, and improves primary patency duration and maturation of murine arteriovenous fistula. J Am Soc Nephrol. 2020;31:931–945 [PubMed: 32152232]
9. Wong C, Bezhaeva T, Rothuizen TC, Metselaar JM, de Vries MR, Verbeek FP, Vahrmeijer AL, Wezel A, van Zonneveld AJ, Rabelink TJ, Quax PH, Rotmans JI. Liposomal prednisolone inhibits vascular inflammation and enhances venous outward remodeling in a murine arteriovenous fistula model. Sci Rep. 2016;6:30439 [PubMed: 27460883]
10. Bezhaeva T, Wong C, de Vries MR, van der Veer EP, van Alem CMA, Que I, Lalai RA, van Zonneveld AJ, Rotmans JI, Quax PHA. Deficiency of tlr4 homologue rp105 aggravates outward remodeling in a murine model of arteriovenous fistula failure. Sci Rep. 2017;7:10269 [PubMed: 28860634]
11. Stirbu O, Gadalean F, Pitea IV, Ciobanu G, Schiller A, Grosu I, Nes A, Bratescu R, Olariu N, Timar B, Tandrau MC. C-reactive protein as a prognostic risk factor for loss of arteriovenous fistula patency in hemodialyzed patients. J Vasc Surg. 2019;70:208–215 [PubMed: 30792061]
12. Kaygin MA, Halici U, Aydin A, Dag O, Binici DN, Limandal HK, Arslan Ü, Kiymaz A, Kahraman N, Calik ES, Savur AI, Erkut B. The relationship between arteriovenous fistula success and inflammation. Ren Fail. 2013;35:1085–1088 [PubMed: 23906289]
13. Lu DY, Chen EY, Wong DJ, Yamamoto K, Protack CD, Williams WT, Assi R, Hall MR, Sadaghianloo N, Dardik A. Vein graft adaptation and fistula maturation in the arterial environment. J Surg Res. 2014;188:162–173 [PubMed: 24582063]
14. Gorecka J, Fereydooni A, Gonzalez L, Lee SR, Liu S, Ono S, Xu J, Liu J, Taniguchi R, Matsubara Y, Gao X, Gao M, Langford J, Yatsula B, Dardik A. Molecular targets for improving arteriovenous fistula maturation and patency. Vasc Investig Ther. 2019;2:33–41
15. Matsubara Y, Kiwan G, Fereydooni A, Langford J, Dardik A. Distinct subsets of t-cells and macrophages impact venous remodeling during arteriovenous fistula maturation. JVS Vasc Sci. 2020
16. Kondo Y, Jadlowiec CC, Muto A, Yi T, Protack C, Collins MJ, Tellides G, Sessa WC, Dardik A. The nogo-b-pirb axis controls macrophage-mediated vascular remodeling. PLoS One. 2013;8:e81019 [PubMed: 24278366]
17. Hoch JR, Stark VK, van Rooijen N, Kim JL, Nutt MP, Warner TF. Macrophage depletion alters vein graft intimal hyperplasia. Surgery. 1999;126:428–437 [PubMed: 10455917]
18. Roy-Chaudhury P, Khan R, Campos B, Wang Y, Kurian M, Lee T, Arend L, Munda R. Pathogenetic role for early focal macrophage infiltration in a pig model of arteriovenous fistula (avf) stenosis. J Vasc Access. 2014;15:25–28 [PubMed: 24043320]
19. Duque JC, Martinez L, Mesa A, Wei Y, Tabbara M, Salman LH, Vazquez-Padron RI. Cd4(+) lymphocytes improve venous blood flow in experimental arteriovenous fistulae. Surgery. 2015;158:529–536 [PubMed: 25999254]
20. Murray PJ, Wynn TA. Protective and pathogenic functions of macrophage subsets. Nat Rev Immunol. 2011;11:723–737 [PubMed: 21997792]
21. Kuwahara G, Hashimoto T, Tsuneki M, Yamamoto K, Assi R, Foster TR, Hanisch JJ, Bai H, Hu H, Protack CD, Hall MR, Schardt JS, Jay SM, Madri JA, Kodama S, Dardik A. Cd44 promotes

inflammation and extracellular matrix production during arteriovenous fistula maturation. Arterioscler Thromb Vasc Biol. 2017;37:1147–1156 [PubMed: 28450292]

22. Guo X, Fereydooni A, Isaji T, Gorecka J, Liu S, Hu H, Ono S, Alozie M, Lee SR, Taniguchi R, Yatsula B, Nassiri N, Zhang L, Dardik A. Inhibition of the akt1-mtorc1 axis alters venous remodeling to improve arteriovenous fistula patency. Sci Rep. 2019;9:11046 [PubMed: 31363142]
23. Mantovani A, Sica A, Sozzani S, Allavena P, Vecchi A, Locati M. The chemokine system in diverse forms of macrophage activation and polarization. Trends Immunol. 2004;25:677–686 [PubMed: 15530839]
24. Rőszer T Understanding the mysterious m2 macrophage through activation markers and effector mechanisms. Mediators Inflamm. 2015;2015:816460 [PubMed: 26089604]
25. Tiemessen MM, Jagger AL, Evans HG, van Herwijnen MJ, John S, Taams LS. Cd4+cd25+foxp3+ regulatory t cells induce alternative activation of human monocytes/macrophages. Proc Natl Acad Sci U S A. 2007;104:19446–19451 [PubMed: 18042719]
26. Agarwal A, Ally W, Brayman K. The future direction and unmet needs of transplant immunosuppression. Expert Rev Clin Pharmacol. 2016;9:873–876 [PubMed: 27043878]
27. Arkwright PD, Motala C, Subramanian H, Spergel J, Schneider LC, Wollenberg A. Management of difficult-to-treat atopic dermatitis. J Allergy Clin Immunol Pract. 2013;1:142–151 [PubMed: 24565453]
28. Chighizola CB, Ong VH, Meroni PL. The use of cyclosporine a in rheumatology: A 2016 comprehensive review. Clin Rev Allergy Immunol. 2017;52:401–423 [PubMed: 27515671]
29. Ferns G, Reidy M, Ross R. Vascular effects of cyclosporine a in vivo and in vitro. Am J Pathol. 1990;137:403–413 [PubMed: 2386202]
30. Navarro-Antolín J, Redondo-Horcajo M, Zaragoza C, Alvarez-Barrientos A, Fernández AP, León-Gómez E, Rodrigo J, Lamas S. Role of peroxynitrite in endothelial damage mediated by cyclosporine a. Free Radic Biol Med. 2007;42:394–403 [PubMed: 17210452]
31. Laws RL, Brooks DR, Amador JJ, Weiner DE, Kaufman JS, Ramírez-Rubio O, Riefkohl A, Scammell MK, López-Pilarte D, Sánchez JM, Parikh CR, McClean MD. Changes in kidney function among nicaraguan sugarcane workers. Int J Occup Environ Health. 2015;21:241–250 [PubMed: 25631575]
32. Rodrigues-Diez R, González-Guerrero C, Ocaña-Salceda C, Rodrigues-Diez RR, Egido J, Ortiz A, Ruiz-Ortega M, Ramos AM. Calcineurin inhibitors cyclosporine a and tacrolimus induce vascular inflammation and endothelial activation through tlr4 signaling. Sci Rep. 2016;6:27915 [PubMed: 27295076]
33. Borel JF, Feurer C, Magnée C, Stähelin H. Effects of the new anti-lymphocytic peptide cyclosporin a in animals. Immunology. 1977;32:1017–1025 [PubMed: 328380]
34. Laupacis A, Keown PA, Ulan RA, McKenzie N, Stiller CR. Cyclosporin a: A powerful immunosuppressant. Can Med Assoc J. 1982;126:1041–1046 [PubMed: 7074504]
35. Fruman DA, Klee CB, Bierer BE, Burakoff SJ. Calcineurin phosphatase activity in t lymphocytes is inhibited by fk 506 and cyclosporin a. Proc Natl Acad Sci U S A. 1992;89:3686–3690 [PubMed: 1373887]
36. Kaldy P, Schmitt-Verhulst AM. Regulation of interferon-gamma mrna in a cytolytic t cell clone: Ca(2+)-induced transcription followed by mrna stabilization through activation of protein kinase c or increase in camp. Eur J Immunol. 1995;25:889–895 [PubMed: 7737290]
37. Kudze T, Ono S, Fereydooni A, Gonzalez L, Isaji T, Hu H, Yatsula B, Taniguchi R, Koizumi J, Nishibe T, Dardik A. Altered hemodynamics during arteriovenous fistula remodeling leads to reduced fistula patency in female mice. JVS Vasc Sci. 2020;1:42–56 [PubMed: 32754721]
38. Yamamoto K, Li X, Shu C, Miyata T, Dardik A. Technical aspects of the mouse aortocaval fistula. J Vis Exp. 2013:e50449 [PubMed: 23892387]
39. Yamamoto K, Protack CD, Tsuneki M, Hall MR, Wong DJ, Lu DY, Assi R, Williams WT, Sadaghianloo N, Bai H, Miyata T, Madri JA, Dardik A. The mouse aortocaval fistula recapitulates human arteriovenous fistula maturation. Am J Physiol Heart Circ Physiol. 2013;305:H1718–1725 [PubMed: 24097429]
40. Hashimoto T, Isaji T, Hu H, Yamamoto K, Bai H, Santana JM, Kuo A, Kuwahara G, Foster TR, Hanisch JJ, Yatsula BA, Sessa WC, Hoshina K, Dardik A. Stimulation of caveolin-1 signaling

improves arteriovenous fistula patency. Arterioscler Thromb Vasc Biol. 2019;39:754–764 [PubMed: 30786746]

41. Protack CD, Foster TR, Hashimoto T, Yamamoto K, Lee MY, Kraehling JR, Bai H, Hu H, Isaji T, Santana JM, Wang M, Sessa WC, Dardik A. Eph-b4 regulates adaptive venous remodeling to improve arteriovenous fistula patency. Sci Rep. 2017;7:15386 [PubMed: 29133876]
42. Hu H, Lee SR, Bai H, Guo J, Hashimoto T, Isaji T, Guo X, Wang T, Wolf K, Liu S, Ono S, Yatsula B, Dardik A. Tgfβ (transforming growth factor-beta)-activated kinase 1 regulates arteriovenous fistula maturation. Arterioscler Thromb Vasc Biol. 2020;40:e203–e213 [PubMed: 32460580]
43. Nakamura K, Kitani A, Strober W. Cell contact-dependent immunosuppression by cd4(+)cd25(+) regulatory t cells is mediated by cell surface-bound transforming growth factor beta. J Exp Med. 2001;194:629–644 [PubMed: 11535631]
44. Green EA, Gorelik L, McGregor CM, Tran EH, Flavell RA. Cd4+cd25+ t regulatory cells control anti-islet cd8+ t cells through tgf-beta-tgf-beta receptor interactions in type 1 diabetes. Proc Natl Acad Sci U S A. 2003;100:10878–10883 [PubMed: 12949259]
45. Amar S, Smith L, Fields GB. Matrix metalloproteinase collagenolysis in health and disease. Biochim Biophys Acta Mol Cell Res. 2017;1864:1940–1951 [PubMed: 28456643]
46. Helin HJ, Edgington TS. Cyclosporin a regulates monocyte/macrophage effector functions by affecting instructor t cells: Inhibition of monocyte procoagulant response to allogeneic stimulation. J Immunol. 1984;132:1074–1076 [PubMed: 6229574]
47. Flores C, Fouquet G, Moura IC, Maciel TT, Hermine O. Lessons to learn from low-dose cyclosporin-a: A new approach for unexpected clinical applications. Front Immunol. 2019;10:588 [PubMed: 30984176]
48. Francis C, Courbon G, Gerber C, Neuburg S, Wang X, Dussold C, Capella M, Qi L, Isakova T, Mehta R, Martin A, Wolf M, David V. Ferric citrate reduces fibroblast growth factor 23 levels and improves renal and cardiac function in a mouse model of chronic kidney disease. Kidney Int. 2019;96:1346–1358 [PubMed: 31668632]
49. Leelahavanichkul A, Huang Y, Hu X, Zhou H, Tsuji T, Chen R, Kopp JB, Schnermann J, Yuen PS, Star RA. Chronic kidney disease worsens sepsis and sepsis-induced acute kidney injury by releasing high mobility group box protein-1. Kidney Int. 2011;80:1198–1211 [PubMed: 21832986]
50. Cheng Y, Zhang F, Zhu J, Wang T, Wei M, Guo D, Mo L, Zhu C, Wang X. Influence of blood pressure variability on the life of arteriovenous fistulae in maintenance hemodialysis patients. Clin Hemorheol Microcirc. 2016;62:129–137 [PubMed: 26444591]
51. Duque JC, Martinez L, Tabbara M, Salman LH, Vazquez-Padron RI, Dejman A. Arteriovenous fistula outcomes in human immunodeficiency virus-positive patients. Saudi J Kidney Dis Transpl. 2018;29:1350–1357 [PubMed: 30588966]
52. Cai C, Kilari S, Singh AK, Zhao C, Simeon ML, Misra A, Li Y, Misra S. Differences in transforming growth factor-β1/bmp7 signaling and venous fibrosis contribute to female sex differences in arteriovenous fistulas. J Am Heart Assoc. 2020;9:e017420 [PubMed: 32757791]

Highlights

- During venous remodeling, T-cells preceded macrophage accumulation in the maturing AVF.
- Inhibition of T-cells reduced macrophage accumulation in the maturing AVF.
- Inhibition of T-cells promoted outward remodeling and reduced vascular wall thickening.
- T-cells regulate macrophage accumulation to regulate adaptive venous remodeling.

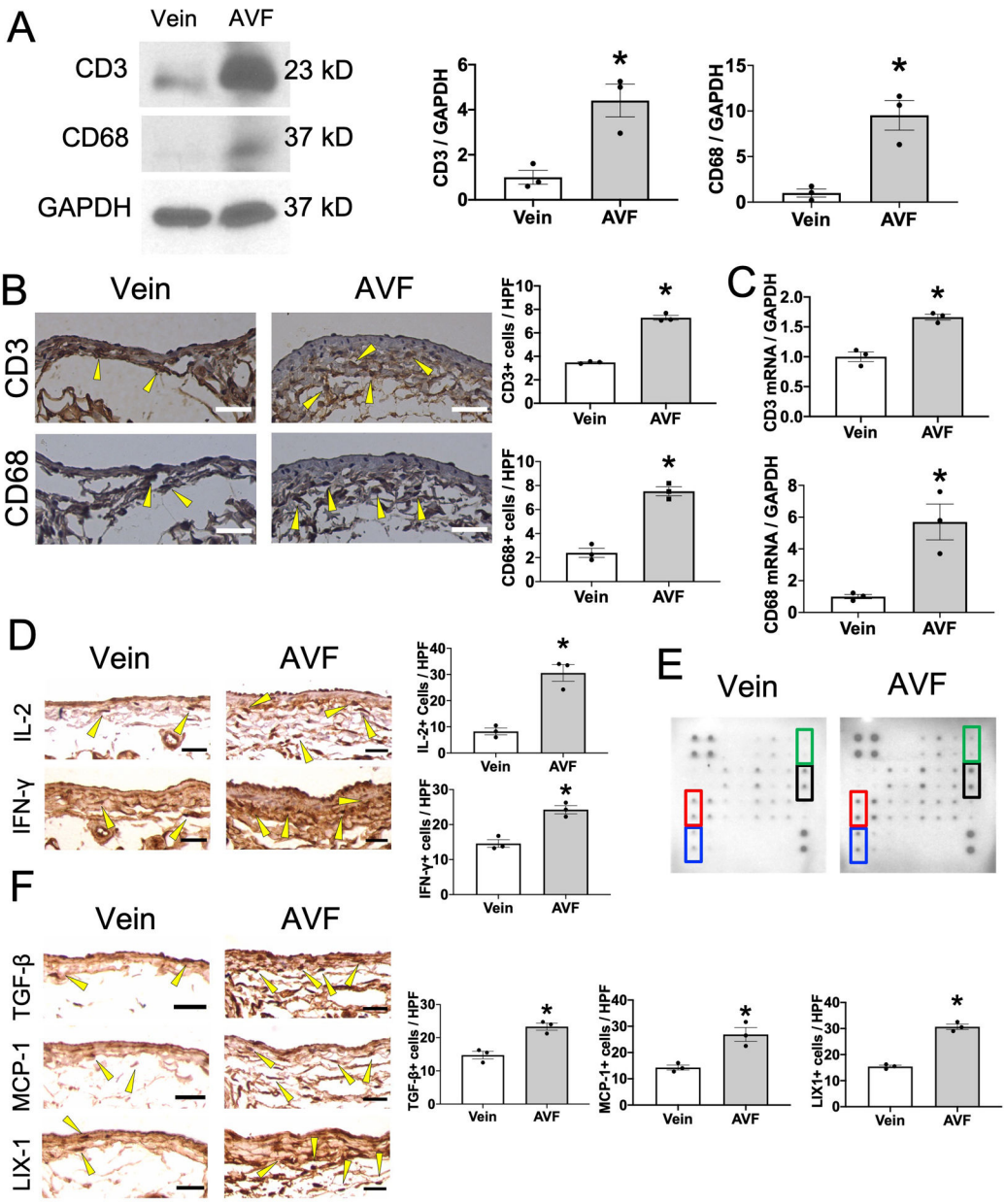

Figure 1. T-cells and macrophages accumulate in the AVF during venous remodeling in wild type mice.

(A) Representative Western blot analysis of CD3, CD68 and GAPDH immunoreactivity in control vein or AVF (day 7). Bar graph shows relative densitometry of CD3 (n=3, *P=0.0126 (t-test), P=0.1000 (Mann-Whitney U test)) and CD68 (n=3, *P=0.0072 (t-test), P=0.1000 (Mann-Whitney U test)). **(B)** Representative photomicrographs showing control vein or AVF (day 7) stained with anti-CD3 or anti-CD68 antibody. Scale bar, 25 μm. Arrowheads show representative CD3- or CD68-positive cells. Bar graphs show quantification of CD3+ cells (n=3, *P<0.0001 (t-test), P=0.1000 (Mann-Whitney U test)) or CD68+ cells (n=3, *P=0.0007 (t-test), P=0.1000 (Mann-Whitney U test)) in the AVF. HPF, high power field. **(C)** Bar graphs show relative number of CD3 (n=3, *P=0.0021 (t-test), P=0.1000 (Mann-Whitney U test)) or CD68 (n=3, *P=0.0144 (t-test), P=0.1000 (Mann-

Whitney U test)) mRNA transcripts in the control vein or AVF (day 7). **(D)** Representative photomicrographs of control vein or AVF (day 7) stained with anti-IL-2 or anti-IFN-γ antibody. Bar graphs show quantification of IL-2+ cells (n=3, *P=0.0029 (t-test), P=0.1000 (Mann-Whitney U test)) or IFN-γ+ cells (n=3, *P=0.0037 (t-test), P=0.1000 (Mann-Whitney U test)) in IVC wall. **(E)** Representative photomicrographs showing the cytokine array examining lysates of control vein or AVF (day 7). Marked cytokines have significant differences between control and AVF. Red, MCP-1; blue, TGF-β; green, IFN-γ; black, LIX1. **(F)** Representative photomicrographs showing control vein or AVF (day 7) stained with anti-TGF-β1, anti-MCP-1 or anti-LIX antibody. Bar graphs show quantification of TGF-β+ cells (n=3, *P=0.0054 (t-test), P=0.1000 (Mann-Whitney U test)), MCP-1+ cells (n=3, *P=0.0109 (t-test), P=0.1000 (Mann-Whitney U test)) or LIX1+ cells (n=3, *P=0.0002 (t-test), P=0.1000 (Mann-Whitney U test)) in the control vein or AVF.

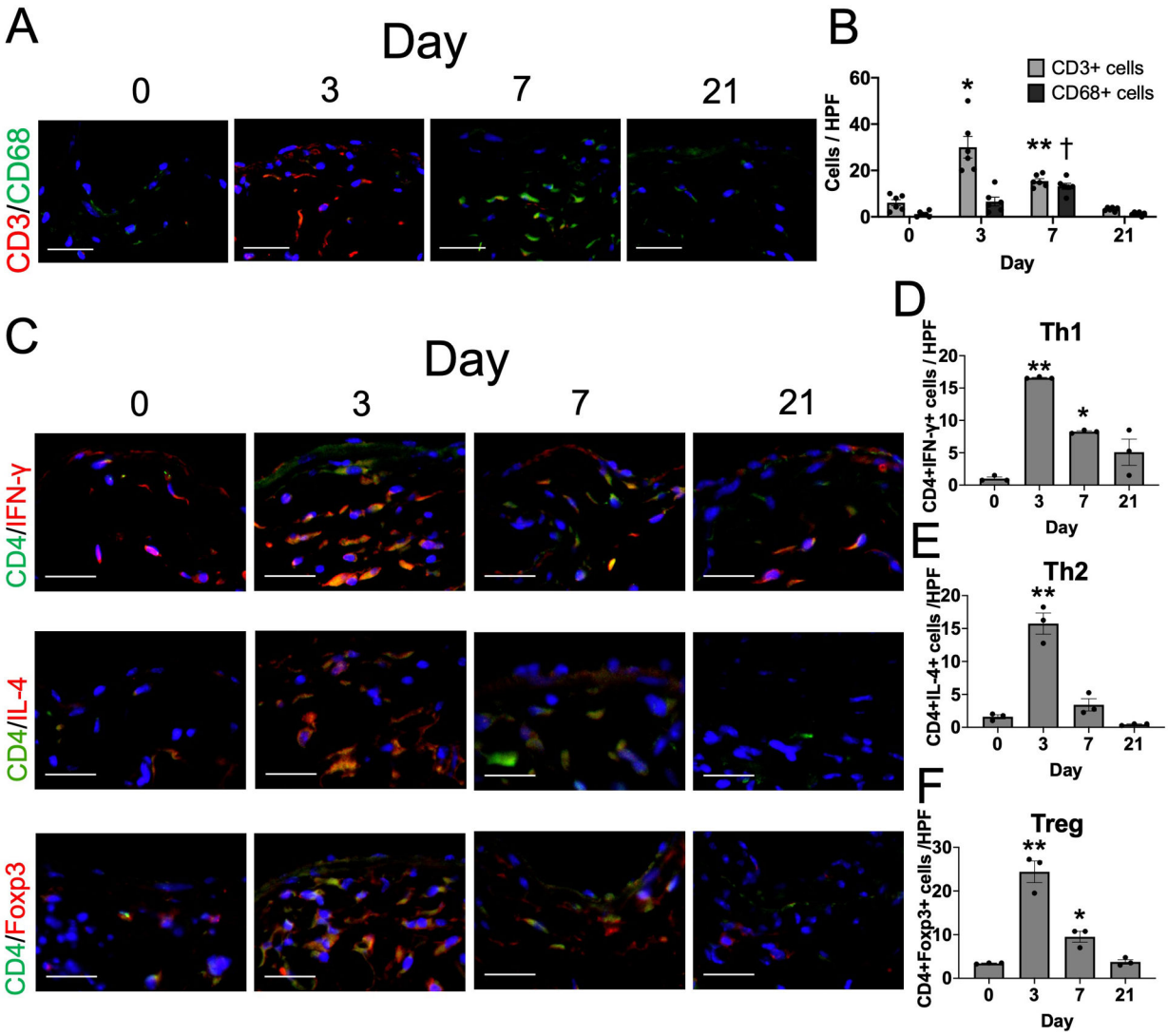

Figure 2. T-cells precede macrophages in the remodeling venous wall in wild type mice.

(A) Representative photomicrographs showing CD3 (red) and CD68 (green) in the AVF wall at days 0, 3, 7 or 21. Scale bar, 50 μm. **(B)** Bar graph shows quantification of CD3- or CD68-positive cells in the AVF at day 0, 3, 7 or 21. n=6. P<0.0001 (2-way ANOVA); *P=0.0076 (day 3 vs day 0, post hoc). **P=0.0002 (day 7 vs day 0, post hoc). †P=0.0003 (day 7 vs day 0, post hoc). **(C)** Representative photomicrographs showing CD4 (green) and IFN-γ (red), CD4 (green) and IL-4 (red) or CD4 (green) and Foxp3 (red) in the AVF wall at days 0, 3, 7 or 21. Scale bar, 50 μm. **(D)** Bar graph shows quantification of CD4+IFN-γ+ cells in the AVF at day 0, 3, 7 or 21. n=3. P<0.0001 (ANOVA), P=0.0017 (Kruskal-Wallis); **P<0.0001 (day 3 vs day 0, post hoc). *P=0.0027 (day 7 vs day 0, post hoc). **(E)** Bar graph shows quantification of CD4+IL-4+ cells in the AVF at day 0, 3, 7 or 21. n=3. P<0.0001 (ANOVA), P<0.0001 (Kruskal-Wallis); **P<0.0001 (day 3 vs day 0, post hoc). **(F)** Bar graph shows quantification of CD4+Foxp3+ cells in the AVF at day 0, 3, 7 or 21. n=3. P<0.0001 (ANOVA), P=0.0012 (Kruskal-Wallis); **P<0.0001 (day 3 vs day 0, post hoc). *P=0.0386 (day 7 vs day 0, post hoc).

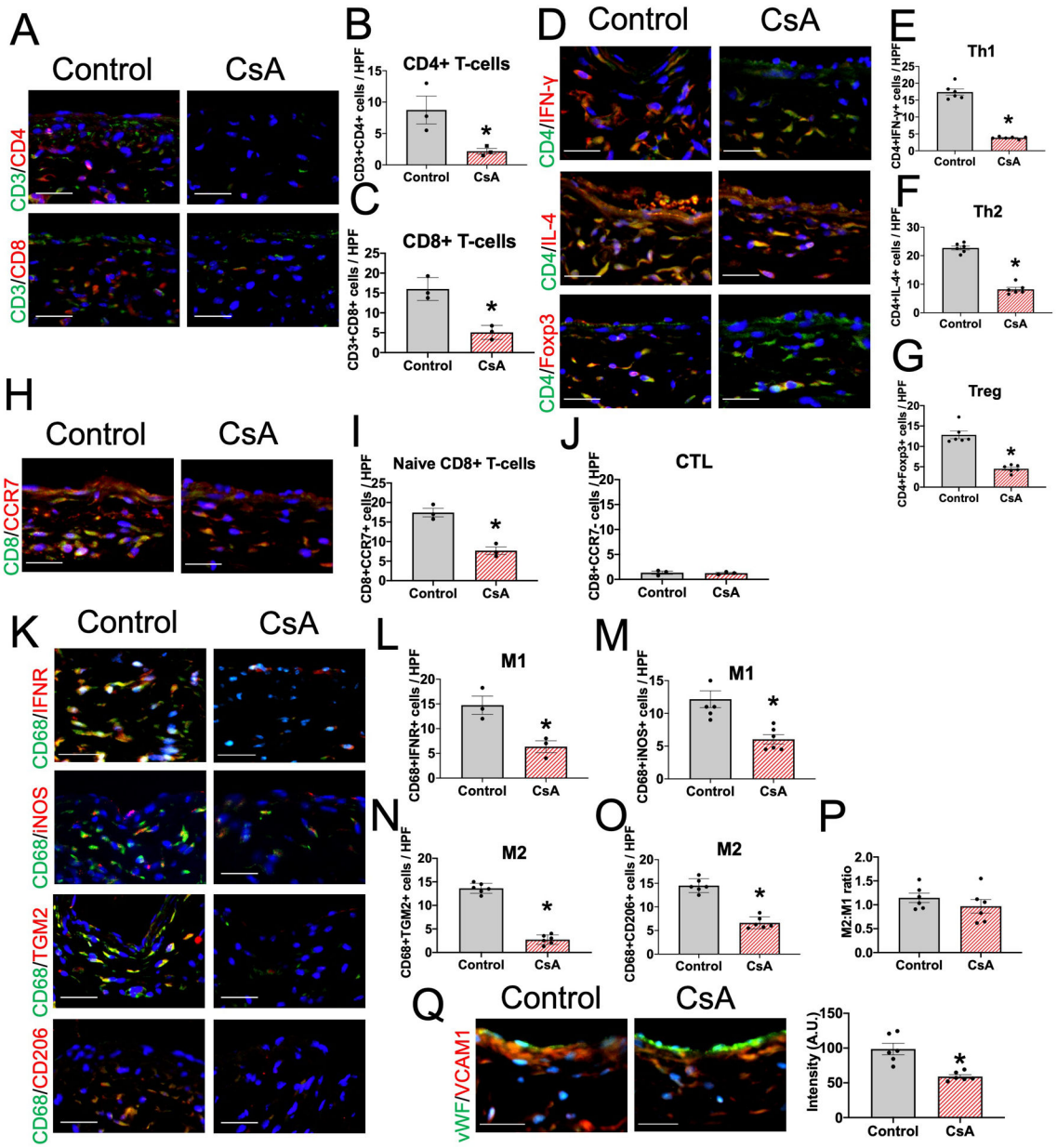

Figure 3. CsA is associated with reduced T-cells and macrophages during venous remodeling in wild type mice.

(A) Representative photomicrographs showing CD3 (green) and CD4 (red) or CD3 (green) and CD8 (red) in the AVF wall (day 7) in mice treated with vehicle (control) or CsA. Scale bar, 50 μm. **(B)** Bar graph shows quantification of CD3+CD4+ cells in the AVF (day 7). n=3. *P=0.0439 (t-test), P=0.1000 (Mann-Whitney U test). **(C)** Bar graph shows quantification of CD3+CD8+ cells in the AVF wall (day 7) in mice treated with control or CsA. n=3. *P=0.0050 (t-test), P=0.1000 (Mann-Whitney U test). **(D)** Representative photomicrographs showing CD4 (green) and IFN-γ (red), CD4 (green) and IL-4 (red) or CD4 (green) and Foxp3 (red) in the AVF wall (day 7) in mice treated with control or CsA. Scale bar, 50 μm. **(E)** Bar graph shows quantification of CD4+IFN-γ+ cells in the AVF (day 7). n=6. *P<0.0001 (t-test). Th1, T-helper type 1 cells. **(F)** Bar graph shows quantification of

CD4+IL-4+ cells in the AVF (day 7). n=6. *P<0.0001 (t-test). Th2, T-helper type 2 cells. **(G)** Bar graph shows quantification of CD4+Foxp3+ cells in the AVF (day 7). n=6. *P<0.0001 (t-test). Treg, regulatory T-cells. **(H)** Representative photomicrographs showing CD8 (green) and CCR7 (red) in the AVF wall (day 7) in mice treated with vehicle control or CsA. Scale bar, 50 μm. **(I)** Bar graph shows quantification of CD8+CCR7+ cells in the AVF (day 7). n=3. *P=0.0026 (t-test), P=0.1000 (Mann-Whitney U test). **(J)** Bar graph shows quantification of CD8+CCR7- cells in the AVF (day 7). n=3. P=0.8149 (t-test), P=0.8000 (Mann-Whitney U test). CTL, cytotoxic T-cells. **(K)** Representative photomicrographs showing CD68 (green) and interferon γ receptor (IFNR; red), CD68 (green) and iNOS (red), CD68 (green) and TGM2 (red) or CD68 (green) and CD206 (red) in the AVF wall (day 7) in mice treated with control or CsA. Scale bar, 50 μm. **(L)** Bar graph shows quantification of CD68+IFNR+ cells in the AVF (day 7). n=3. *P<0.0187 (t-test), P=0.1000 (Mann-Whitney U test). M1, M1 macrophages. **(M)** Bar graph shows quantification of CD68+iNOS+ cells in the AVF (day 7). n=6. *P<0.0001 (t-test). **(N)** Bar graph shows quantification of CD68+TGM2+ cells in the AVF (day 7). n=6. *P<0.0001 (t-test). M2, M2 macrophages. **(O)** Bar graph shows quantification of CD68+CD206+ cells in the AVF (day 7). n=6. *P<0.0001 (t-test). **(P)** Bar graph shows the ratio of M2:M1-type macrophages in the AVF (day 7). n=6. P=0.3303 (t-test). **(Q)** Representative photomicrographs showing vWF (green) and VCAM1 (red) in the AVF wall (day 7) in mice treated with vehicle (control) or CsA. Scale bar, 50 μm. Bar graph shows quantification of VCAM1 intensity in the AVF (day 7). n=6. P=0.0010 (t-test).

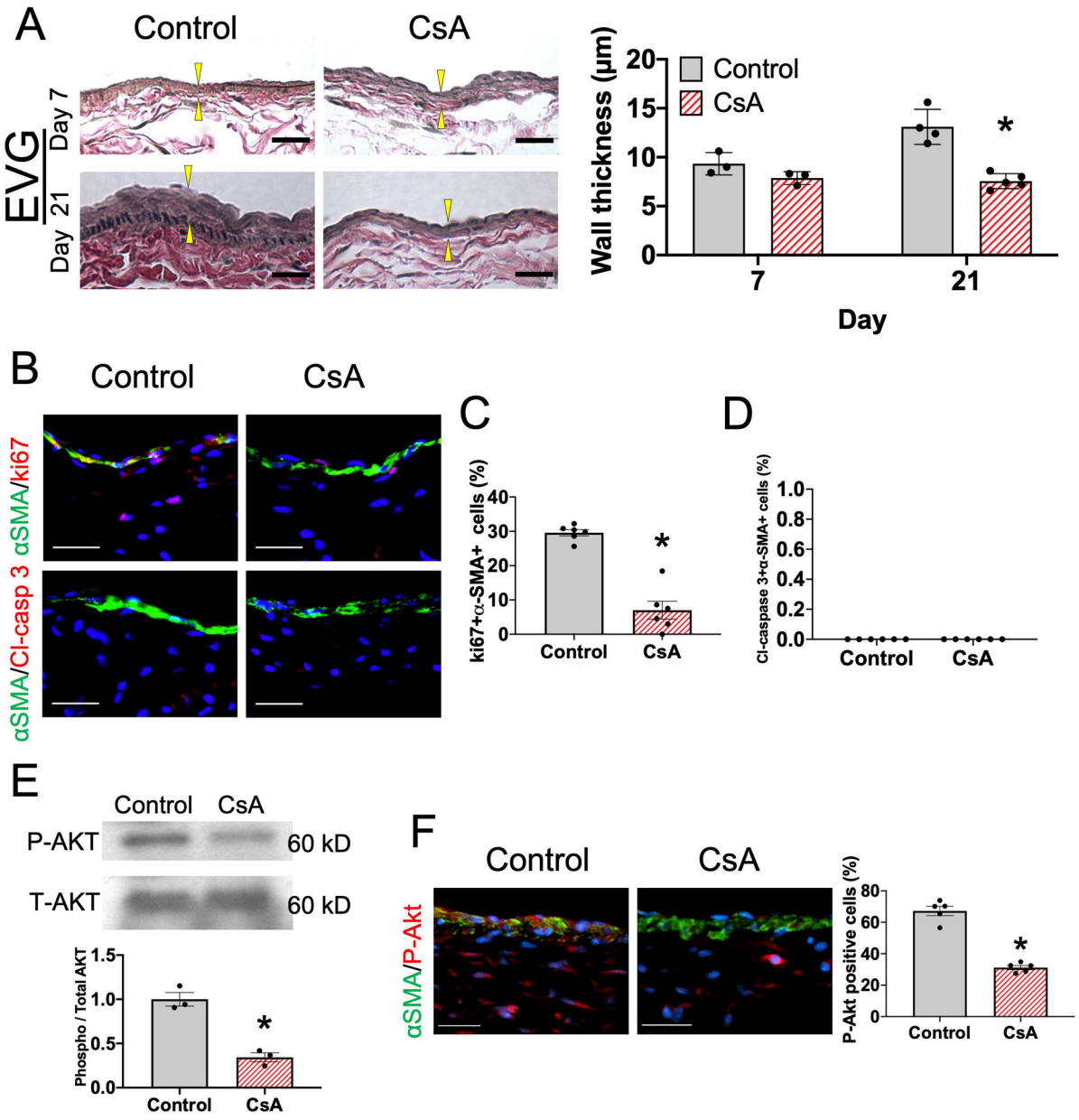

Figure 4. CsA reduces AVF wall thickening and SMC proliferation in wild type male mice.

(A) Representative photomicrographs of the AVF wall of mice treated with vehicle or CsA, stained with Elastin van Gieson (EVG); upper row, day 7; lower row, day 21. Scale bar, 25μm. Arrowheads show intima-media thickness. Bar graph shows intima-media thickness of the AVF wall in mice treated with vehicle (control) or CsA. n=3–5. P=0.0077 (ANOVA). Day 7, P=0.2910 (post hoc). Day 21, *P<0.0001 (post hoc). **(B)** Representative photomicrographs showing α-smooth muscle actin (α-SMA; green) and ki67 (red) or α-SMA (green) and cleaved caspase (Cl-casp) 3 in the AVF wall (day 7) in mice treated with vehicle (control) or CsA. Scale bar, 50 μm. **(C)** Bar graph shows percentage of α-SMA +ki67+ cells in the AVF (day 7). n=6. *P<0.0001 (t-test). **(D)** Bar graph shows percentage of α-SMA+ Cl-casp 3+ cells in the AVF (day 7). n=6. **(E)** Representative Western blot analysis

of phospho-Akt (P-Akt) and total Akt (T-Akt) immunoreactivity in the AVF wall (day 7) in mice treated with control or CsA; bar graph shows relative densitometry of phosphorylated Akt (n=3, *P=0.0021 (t-test), P=0.1000 (Mann-Whitney U test)). **(F)** Representative photomicrographs showing α-SMA (green) and phosphorylated Akt (red) in the AVF wall (day 7) in mice treated with control or CsA. Scale bar, 50 μm. Bar graph shows percentage of α-SMA+P-Akt+ cells in the AVF wall (day 7). n=5. *P<0.0001 (t-test), P=0.0079 (Mann-Whitney U test).

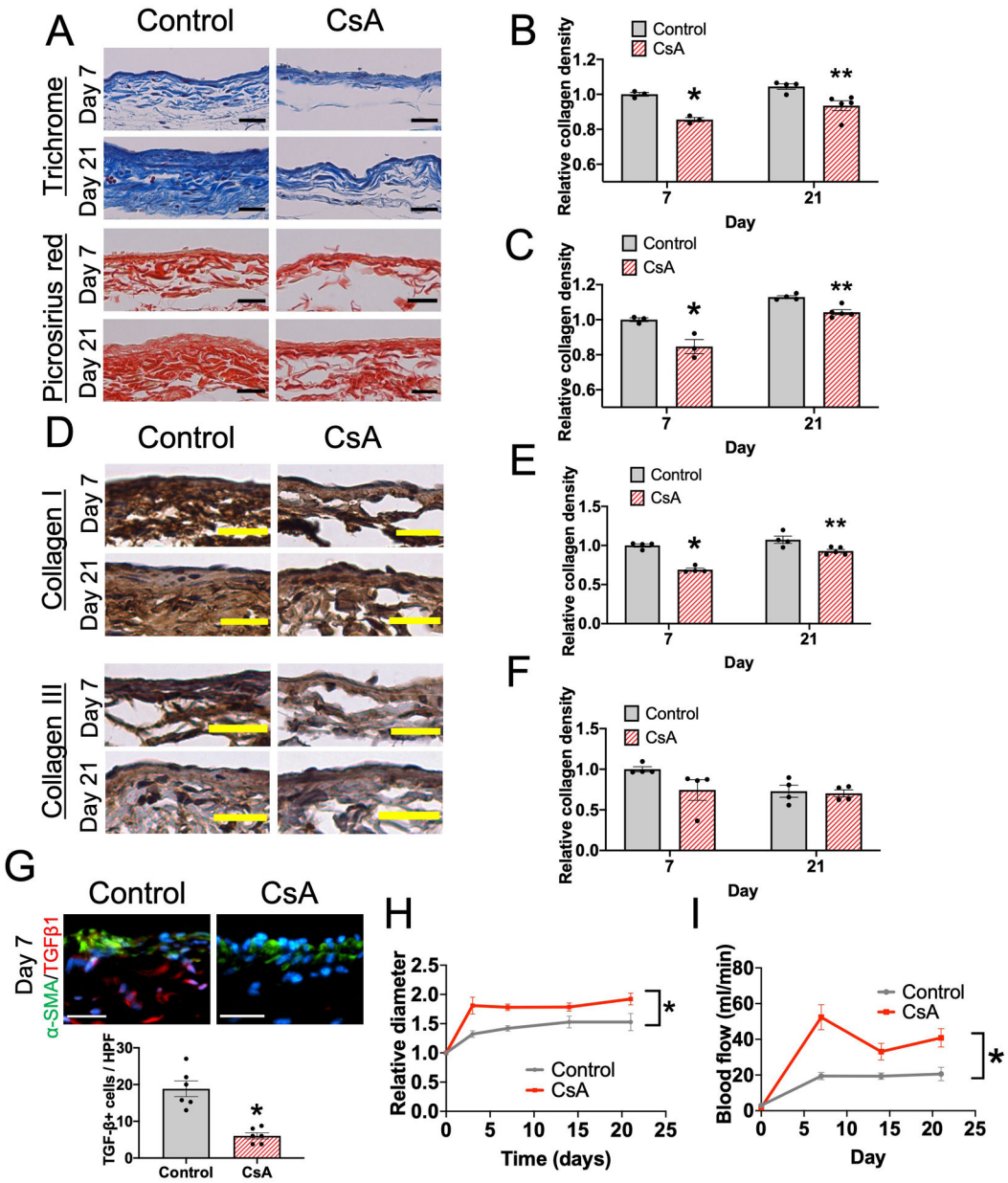

Figure 5. CsA reduces TGF-β expression and collagen density to promote AVF outward remodeling in wild type mice.

(A) Representative photomicrographs of the AVF wall (days 7 and 21) in mice treated with vehicle (control) or CsA; upper panels, Masson trichrome stain; lower panels, picrosirius red stain. Scale bar, 25 μm. **(B)** Bar graph shows relative collagen density in the Masson trichrome stained AVF wall, normalized to the control group (day 7). n=3–5. P=0.0028 (ANOVA). Day 7, *P=0.0051 (post hoc). Day 21, **P<0.0066 (post hoc). **(C)** Bar graph shows relative collagen density in the picrosirius red stained AVF wall, normalized to the control group (day 7). n=3–5. P<0.0001 (ANOVA). Day 7, *P=0.0007 (post hoc). Day 21, **P<0.0108 (post hoc). **(D)** Representative photomicrographs of the AVF wall (days 7 and 21) in mice treated with control or CsA stained with anti-collagen I or anti-collagen III antibody. Scale bar, 25 μm. **(E)** Bar graph shows relative collagen I density in the AVF wall,

normalized to the control group (day 7). n=4–5. P=0.0002 (ANOVA). Day 7, *P<0.0001 (post hoc). Day 21, **P<0.0054 (post hoc). **(F)** Bar graph shows relative collagen III density in the AVF wall, normalized to the control group (day 7). n=4–5. P=0.2352 (ANOVA). **(G)** Representative photomicrographs showing α-SMA (green) and TGFβ1 (red) in the AVF wall (day 7) in mice treated with control or CsA. Scale bar, 50 μm. Bar graph shows quantification of TGFβ1+ cells in the AVF (day 7). n=6. *P<0.0002 (t-test). **(H)** Line graph shows relative AVF diameter of mice treated with control or CsA, normalized to day 0. n=20. *P<0.0001 (ANOVA). Day 3, P<0.0001 (post hoc). Day 7, P<0.0001 (post hoc). Day 14, P=0.0771 (post hoc). Day 21, P=0.0020 (post hoc). **(I)** Line graph shows blood flow within the mouse AVF treated with control or CsA. n=8–13. *P<0.0001 (ANOVA). Day 3, P=0.2223 (post hoc). Day 7, P=0.0020 (post hoc). Day 14, P=0.0760 (post hoc). Day 21, P=0.0626 (post hoc).

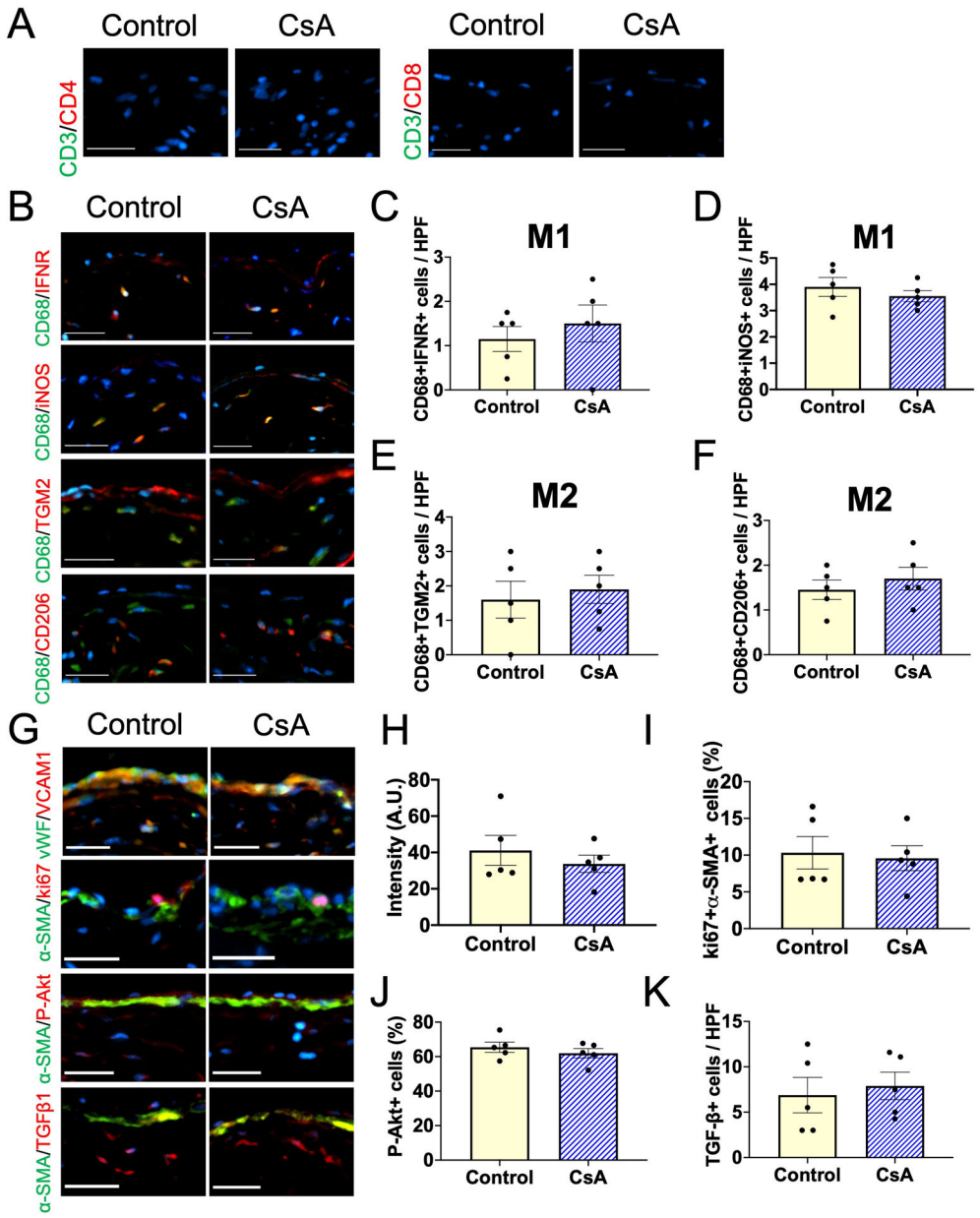

Figure 6. Effects of CsA on AVF macrophage accumulation and SMC proliferation are lost in nude mice.

(A) Representative photomicrographs showing CD3 (green) and CD4 (red) or CD3 (green) and CD8 (red) in the AVF wall (day 7) in nude mice treated with vehicle (control) or CsA. Scale bar, 50 μm. **(B)** Representative photomicrographs showing CD68 (green) and IFNR (red), CD68 (green) and iNOS (red), CD68 (green) and TGM2 (red) or CD68 (green) and CD206 (red) in the AVF wall (day 7) in nude mice treated with control or CsA. Scale bar, 50 μm. **(C)** Bar graph shows quantification of CD68+IFNR+ cells in the AVF (day 7). n=5. P=0.5068 (t-test), P=0.5556 (Mann-Whitney U test). **(D)** Bar graph shows quantification of CD68+iNOS+ cells in the AVF (day 7). n=5. P=0.4271 (t-test), P=0.4603 (Mann-Whitney U test). **(E)** Bar graph shows quantification of CD68+TGM2+ cells in the AVF (day 7). n=5. P=0.6670 (t-test), P=0.8333 (Mann-Whitney U test). **(F)** Bar graph shows quantification of

CD68+CD206+ cells in the AVF (day 7). n=5. P=0.4750 (t-test), P=0.5794 (Mann-Whitney U test). **(G)** Representative photomicrographs showing vWF (green) and VCAM1 (red), α-SMA (green) and ki67 (red), α-SMA (green) and phosphorylated Akt (red) or α-SMA (green) and TGFβ1 (red) in the AVF wall (day 7) in nude mice treated with control or CsA. Scale bar, 50 μm. **(H)** Bar graph shows quantification of VCAM1 intensity in the AVF wall (day 7). n=5. P=0.4613 (t-test), P=0.9999 (Mann-Whitney U test). **(I)** Bar graph shows percentage of α-SMA+ki67+ cells in the AVF wall (day 7). n=5. P=0.7975 (t-test), P=0.9524 (Mann-Whitney U test). **(J)** Bar graph shows percentage of α-SMA +phosphorylated Akt+ cells in the AVF wall (day 7). n=5. P=0.6667 (t-test), P=0.8333 (Mann-Whitney U test). **(K)** Bar graph shows quantification of TGFβ1+ cells in the AVF wall (day 7). n=5. P=0.6931 (t-test), P=0.6349 (Mann-Whitney U test).

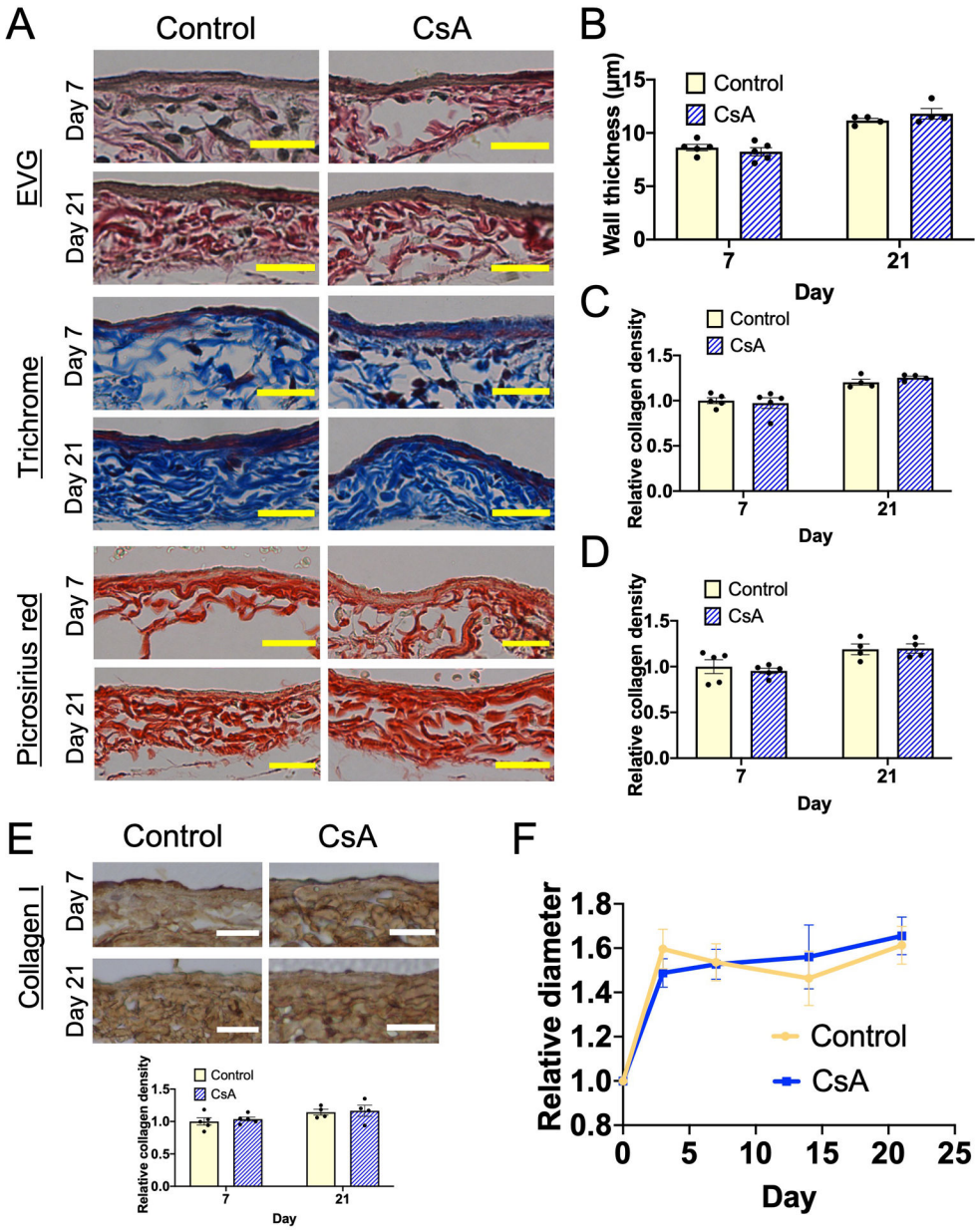

Figure 7. Effects of CsA on AVF wall thickening and adaptive remodeling are lost in nude mice.

(A) Representative photomicrographs of the AVF wall (days 7 and 21) in mice treated with vehicle (control) or cyclosporine (CsA); upper panels, Elastin van Gieson (EVG); middle panels, Masson trichrome stain; lower panels, picrosirius red stain. Scale bar, 25 μm. **(B)** Bar graph shows intima-media thickness of the AVF wall in mice treated with control or CsA. n=4–5. P=0.6575 (ANOVA). Day 7, P=0.6666 (post hoc). Day 21, P=0.2385 (post hoc) **(C)** Bar graph shows relative collagen density in the Masson trichrome stained AVF wall in nude mice treated with control or CsA, normalized to the control group (day 7). n=4–5. P=0.7690 (ANOVA). Day 7, P=0.8680 (post hoc). Day 21, P=0.6619 (post hoc). **(D)** Bar graph shows relative collagen density in the picrosirius red stained AVF wall in nude mice treated with control or CsA, normalized to the control group (day 7). n=4–5. P=7132 (ANOVA). Day 7,

P=0.7994 (post hoc). Day 21, P=0.9988 (post hoc). **(E)** Representative photomicrographs of the AVF wall (days 7 and 21) in nude mice treated with control or CsA stained with anti-collagen I antibody. Scale bar, 25 μm. Bar graph shows relative collagen I density in the AVF wall, normalized to the control group (day 7). n=5. P=0.8608 (ANOVA). **(F)** Line graph shows relative AVF diameter of nude mice treated with vehicle (control) or CsA, normalized to day 0. n=10. P=0.8241 (group factor, ANOVA). Day 3, P=0.6643 (post hoc). Day 7, P=0.9732 (post hoc). Day 14, P=0.8424 (post hoc). Day 21, P=0.9996 (post hoc).

Table.

Relative cytokine expression in AVF measured by cytokine array

		Relative cytokine expression	P value
Growth factors	IGF-1	0.36	0.3978
	TGF-β	1.59	0.0009
	VEGF	1.86	0.2674
Chemokines	MCP-1	1.59	0.0098
	M-CSF	1.92	0.0816
	MIP-1α	2.89	0.0631
	Fractalkine	1.76	0.0563
	RAGE	1.28	0.5312
	GCSF	1.11	0.8062
	KC	1.86	0.2337
	TARC	1.77	0.1991
	LIX	2.11	0.0107
	SDF-1α	1.16	0.8178
Protease	MMP-2	3.56	0.1774
	MMP-3	1.55	0.2945
Cytokines	Fas Ligand	1.17	0.6160
	TNF-α	1.76	0.2626
	IFN-γ	2.91	0.0244
	IL-1α	1.9	0.1677
	IL-1β	1.86	0.1562
	IL-4	1.25	0.4690
	IL-6	1.71	0.3753
	IL-10	0.83	0.6320

IGF, insulin like growth factor; TGF-β, transforming growth factor-beta; VEGF, vascular endothelial growth factor; MCP-1, monocyte chemotactic protein-1; M-CSF, macrophage colony-stimulating factor; MIP-1α, Macrophage inflammatory protein-1 alpha; RAGE, receptor for advanced glycation end products; GCSF, granulocyte-colony stimulating factor; KC, keratinocyte chemoattractant; TARC, thymus and activation-regulated chemokine; LIX, lipopolysaccharide-induced CXC chemokine; SDF-1α, stromal cell-derived factor-1 alpha; MMP, matrix metalloproteinase; TNF-α, tumor necrosis factor-alpha; IFN-γ, interferon-gamma; IL, interleukin.